



Investigation on Thermal Behavior During Pressurization Discharge of Liquid Oxygen Under Different Acceleration Levels

Zhan Liu¹ · Xin Yin¹ · Yuanliang Liu¹ · Yanzhong Li²

Received: 10 November 2021 / Accepted: 21 March 2022 / Published online: 29 April 2022
© The Author(s) 2022

Abstract

Cryogenic pressurization discharge involves on complex heat exchange and fluid flow issues, and the related thermal physical performance should be comprehensively investigated. In this study, a two-dimensional axisymmetric numerical model is adopted to research the outflow characteristic from a cylindrical liquid oxygen storage tank with the gas injection. The VOF method is utilized to predict the pressurization discharge with 360 K high-temperature gaseous oxygen as the pressurant gas. Validated against the liquid hydrogen discharge experiments, the numerical model is turned out to be proper and acceptable with the calculation errors limited within 20%. On the basis of the numerical model, effect of the flight acceleration level on the tank pressurization and liquid outflow performance are numerically simulated and analyzed, with the gas injection rate of 0.18 kg/s and the liquid outflow rate of 36.0 kg/s. Some valuable conclusions are obtained finally. The present study is significant to the safety flight of launch vehicle and may supply some technical supports for the design of cryogenic propellant system.

Keywords Thermal behavior · Pressurization discharge · Gas injection · Liquid outflow · Acceleration level

Introduction

Cryogenic propellants, including liquid hydrogen and liquid oxygen (Wang et al. 2020; Suñol et al. 2020; Li et al. 2022; Chen et al. 2022), are widely used as power fuel on aerospace engineering and deep space exploration (Inoue et al. 2021; Liu et al. 2019a, b). The launch system experiences variable dynamic accelerations during liftoff and ballistic flight, which usually brings serious safety issues on the thermal behavior within cryogenic fuel storage tanks. To improve the liftoff stability and operation safety of cryogenic launch system, the heat transfer and phase change phenomenon involved in the pressurization discharge should be deeply investigated.

Focused on the gas injection and drainage of cryogenic fluids, investigators conducted large amount of researches, including the experimental test and numerical simulation. In the 1960s', Stochl et al. (1969, 1970a, b) conducted the pressurized outflow experiment from a liquid hydrogen tank. Both the gaseous helium and gaseous hydrogen were used as pressurant gas. The effects of the outflow mass rate, gas injection flow rate, and initial parameter settings on the liquid outflow were experimentally researched. Aydelott (1967a) investigated the self-pressurization performance in a liquid hydrogen tank by conducting a series of transient tests. Different influence factors, including the liquid height, heating mode and tank structure, were studied. Based on the measured results, Aydelott (1967b) theoretically analyzed the tank pressure rise in low gravity levels. They found that compared to micro-gravity condition, the tank pressure rise was much faster in normal gravity. Van Dresar and Stochl (1991, 1993) conducted some pressurized discharge experiments in low gravity and in normal gravity. The results showed that the pressurant gas consumption was greatly related to the heat exchange among the ullage, the liquid, the tank wall, and the injected gas. Ludwig and Dreyer (2014) established a ground experimental rig to research the active-pressurization performance in a liquid nitrogen tank.

✉ Zhan Liu
liuzhankd@cumt.edu.cn

¹ State Key Laboratory for Geomechanics and Deep Underground Engineering, School of Mechanics and Civil Engineering, China University of Mining and Technology, Xuzhou 221116, China

² School of Energy and Power Engineering, Xi'an Jiaotong University, Xi'an 710049, China

The gaseous nitrogen and gaseous helium were adopted as pressurant gas. The thermal physical performance, including the fluid stratification, tank pressure rise, and pressurant gas consumption, were experimentally researched during active pressurization.

Researchers also developed different models, and adopted different treatments to predict the pressurized discharge from cryogenic fuel storage tanks. Roudebush (1965) developed a 1-dimensional calculation model to research the liquid outflow performance with considering the thermal stratification in the ullage. Mandell and Roudebush (1965) made some corrections on the Roudebush model, to improve the prediction accuracy and extend the application range. Hochstein et al. (1990) developed a SOLA-ECLIPSE program to simulate the tank self-pressurization with consideration of different heat transfer methods. They found that the liquid subcooling could significantly reduce the tank pressure rise rate and is beneficial to the long-term storage of cryogenics. Hearn (2001) and Majumdar and Steadman (2001) developed a lumped parameter model to research the outflow of cryogenics. Panzarella and Kassemi (2005) considered the liquid flow and fluid temperature variation, and proposed a lumped thermodynamic numerical model to predict the tank pressurization under microgravity conditions. The simulated results showed that even in low gravity conditions, the thermal buoyancy and natural convection also cause obvious effects on the phase distribution. Barsi and Kassemi (2008) developed a numerical model to simulate the self-pressurization in a partially full liquid hydrogen tank. The results showed that the developed two-phase numerical model was in good agreement with the measured results. Seo and Jeong (2010) considered different heat transfer modes and proposed a thermal diffusion model to study the self-pressurization in a cryogenic fuel storage tank. Wang et al. (2013, 2015) numerically investigated the pressurization performance in a liquid oxygen tank during liftoff. The tank pressurization and fluid outflow were investigated and compared under different influence factors, including the pressurant gas, the injected gas temperature, and the thickness of the tank wall. Liu et al. (2016) established a numerical model and researched the liquid outflow performance during space-entering phase. Both the liquid discharge and fluid thermal stratification were greatly predicted under the effect of space radiation. To study the complex heat exchange during the pressurized discharge, Li et al. (2019) developed a 2D axial symmetry numerical model to simulate the thermal physical process in a spherical liquid hydrogen tank with gaseous helium and gaseous hydrogen as pressurant gas. Researchers compared and analyzed effects of the gas temperature, outflow rate and pressurant gas on the tank pressurization and liquid outflow characteristic. They found that the pressurant gas consumption is directly related to the heat transfer modes within the tank.

Although researchers have conducted several experimental tests and numerical investigations on the pressurization discharge of cryogen, the effect of the flight acceleration, especially the super gravity level, on the liquid outflow was few involved. Based on the pervious researches, a 2-dimensional axisymmetric model is adopted to research the outflow characteristic of liquid oxygen from an aerospace fuel storage tank. The high-temperature gaseous oxygen is used as the pressurant gas. The influence of the flight acceleration on the tank pressurization and liquid outflow are simulated and analyzed. This study is beneficial to deeply understand the thermodynamic behavior during the pressurization discharge, and some interesting findings may supply useful guidance on the optimal design of cryogenic launch system.

Research Object

As Fig. 1 shows, a liquid oxygen tank (Liu et al. 2016), made of 2.4 mm-thickness 2219 aluminum alloy, is selected to study the thermodynamic performance during liftoff. The tank consists of a cylinder and two elliptical heads, and covers with a foam layer. The thickness of foam 1 varies from 20 to 80 mm, and the thickness of foam 2 is 20 mm. The thermophysical properties of the tank wall and foam layers are listed in Table 1. The detailed tank geometry parameters are marked in Fig. 1. The initial liquid height is 2.962 m, and the initial masses of the liquid and gas are 12,309.0 kg

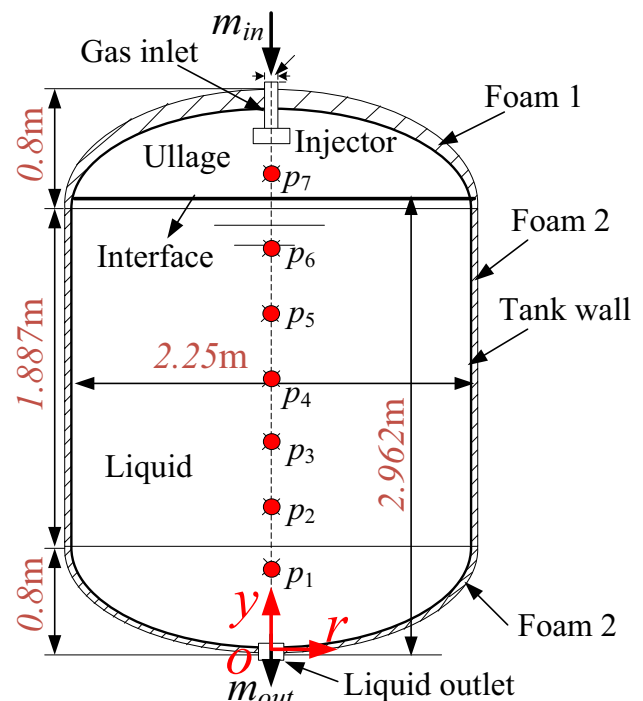


Fig. 1 Diagram of liquid oxygen tank (Liu et al. 2016)

Table 1 Thermal properties of foam

Parameter	Density	Heat capacity	Thermal conductivity
Tank wall	2800 kg/m ³	830 J/(kgK)	159 W/(mK)
Foam 1	75 kg/m ³	1000 J/(kgK)	$\lambda = 0.01319 + 1.4365 \times 10^{-7}T + 1.587 \times 10^{-7}T^2$
Foam 2	40 kg/m ³	1470 J/(kgK)	0.03 W/(mK)

and 24.5 kg. The ambient pressure is about 85.495 kPa. As the tank experiences long-term ground parking, the liquid temperature almost reaches the saturation temperature corresponding to the ambient pressure with the value of 88.6 K. Once the storage tank is locked, the high-temperature gas is injected and used to increase the tank pressure. While the tank pressure reaches to 400 kPa, the liquid is discharged. The initial gas temperature is set as 300 K. The gas diffuser and liquid outlet are located in the top and bottom elliptical head. For the fuel storage tank of an upper stage, 360 K gaseous oxygen is adopted as the pressurant gas and is injected into the tank with the mass flow rate of 0.18 kg/s. The out-flow mass rate is 36.0 kg/s, under the effect of a turbo pump.

Numerical Model

Governing Equation

As the present numerical simulation involves on the heat exchange, gas injection and fluid drainage, the basic governing equations are given.

$$\frac{1}{\rho_q} \left[\frac{\partial}{\partial t} (\alpha_q \rho_q) + \nabla \cdot (\alpha_q \rho_q \vec{v}_q) \right] = \frac{1}{\rho_q} S_m \tag{1}$$

$$\frac{\partial}{\partial t} (\rho \vec{v}) + \nabla \cdot (\rho \vec{v} \vec{v}) = -\nabla p + \nabla \cdot [\mu (\nabla \vec{v} + \nabla \vec{v}^T)] + \rho \vec{g} + \vec{F}_{vol} \tag{2}$$

$$\frac{\partial}{\partial t} (\rho E) + \nabla \cdot (\vec{v} (\rho E + p)) = \nabla \cdot (\lambda \nabla T) + S_h \tag{3}$$

The volume of fluid (VOF) method is adopted to predict the distribution and location of the interface. In each cell, the liquid volume fraction α_L and gas volume fraction α_V sums to unity. The fluid density, viscosity and thermal conductivity are calculated in terms of volume fraction. The energy term is calculated by the mass-averaged variables. The continuous surface force model is used to simulate the surface tension, which is reflected as a volume force in the momentum equation.

Moreover, in the numerical model, the liquid density is treated with Boussinesq approximation $\rho \approx \rho_0 [1 - \beta(T - T_0)]$. Here, ρ_0 means the reference density at temperature of T_0 . As the thermal expansion coefficient of

the liquid is not sensitive to fluid pressure and varies small in the present temperature range, it is set with constant value of 0.0043 1/K. The initial liquid density is 1149.1 kg/m³. The gaseous oxygen is modeled as the ideal gas. The specific heat values of liquid oxygen and gaseous oxygen are 1695.3 J/(kg K) and 924.54 J/(kg K), and the thermal conductivity values of liquid oxygen and gaseous oxygen 0.15308 W/(m K) and 0.02662 W/(m K).

Phase Change Model

Influenced by external heat leak and heat exchange from the gas to the liquid, the phase change inevitably occurs at the interface. Here, the Lee’s phase change model (Lee 1980) is adopted. The phase change is assumed to occur at a constant pressure and at a quasi thermo-equilibrium state, and mainly dependent on the saturation temperature T_{SAT} . When $T_L > T_{SAT}$, the liquid evaporates, and when $T_G < T_{SAT}$, the gas condenses. The energy source term S_h is the product of the mass transfer term S_m and the latent heat h_{fg} .

$$S_m = \begin{cases} r_L \alpha_L \rho_L (T_L - T_{SAT}) / T_{SAT} & T_L > T_{SAT} \\ r_G \alpha_G \rho_G (T_{SAT} - T_G) / T_{SAT} & T_G < T_{SAT} \end{cases} \tag{4}$$

$$S_h = S_m h_{fg} \tag{5}$$

where, r_L and r_G refer to the mass transfer intensity factor. The value of 0.1 s⁻¹ has been validated for the heat transfer issues on cryogenics by different investigators (Liu et al. 2020a, b, 2021, 2022; Mao et al. 2021; Wickert and Prokop 2021; Liu and Li 2021). Moreover, as the saturation temperature of liquid oxygen varies with the tank pressure, both parameters are updated with time. Two parameters are obtained from the thermal physical software REFPROP (NIST Chemistry WebBook 2011), and fitted as $T_{SAT} = 82.331 + 8.697e^{-5}p - 6.980e^{-11}p^2$. The fitted equation is implanted into the numerical model to reflect variations of the fluid pressure and phase change temperature during the whole process.

Calculation Setting

For the present liquid oxygen tank, a two-dimensional axial symmetry numerical model is established. The cylinder, foam layer and tank wall are divided into structured grids,

Table 2 Initial setting of three conditions (Stochl et al. 1969; Roudebush 1965)

Case No	Pressure	Outflow time	Outflow rate	Gas temperature	Liquid height
1	280 kPa	87 s	7.22 L/s	Linearly vary within 24.4-214 K	0.15 m
2	390 kPa	283 s	2.21 L/s	Linearly vary within 26.1-207 K	0.15 m
3	400 kPa	100 s	6.34 L/s	Linearly vary within 26.1-221 K	0.11 m

while the up and bottom elliptical head are generated with unstructured grids. The ANSYS Fluent 19.0 is utilized to simulate the thermal physical process with double precision solver. The geometric reconstruction scheme is adopted. The convective term is discretized by the second-order upwind scheme. The PISO pressure–velocity coupling scheme is adopted. During the numerical simulation, the value of the Cr number is limited within 5.0. The time discretization is used by the explicit first order scheme.

While the liquid oxygen tank is in the ground parking, the convection heat transfer coefficients of the cylinder section is about $22 \text{ W}/(\text{m}^2 \text{ K})$ (Liu et al. 2017) with the coming air velocity of 10 m/s and air temperature of 293 K , and the corresponding heat flux through the cylinder section is about $280 \text{ W}/\text{m}^2$. With the initial liquid height of 2.962 m , the value of the dimensionless Rayleigh number ($Ra^* = g_0 \beta \rho^2 c_p q l^4 / (\mu \lambda^2)$) could reach 10^{20} . It means the natural convection close to the tank wall is in turbulent flow, the $k - \epsilon$ turbulent model is therefore adopted to predict the pressurization discharge of liquid oxygen. The model constants are $C_\mu = 0.09$, $\sigma_k = 1.0$, $\sigma_\epsilon = 1.3$, $C_{1\epsilon} = 1.44$ and $C_{2\epsilon} = 1.92$. The detailed descriptions on the $k - \epsilon$ turbulent model could refer to the related investigations (Liu et al. 2016).

Model Validation

The fluid outflow tests conducted by the Lewis Research Center (Stochl et al. 1969; Roudebush 1965) are selected

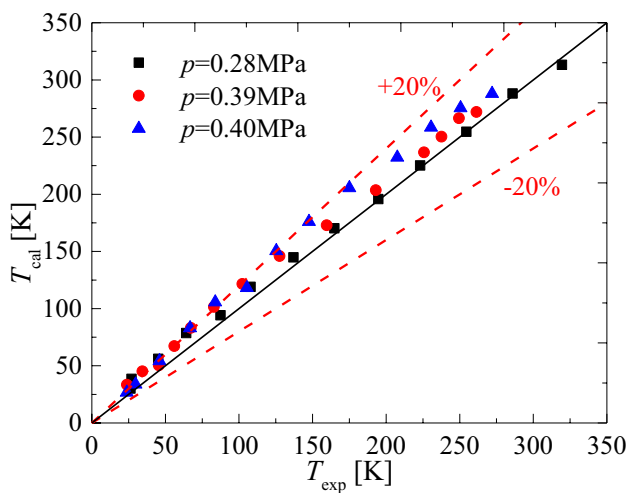


Fig. 2 Numerical model validation against experimental results (Stochl et al. 1969; Roudebush 1965)

to validate the present numerical model. The experiments were conducted in a cylindrical liquid hydrogen tank. Three experimental cases with the tank pressure of 280 kPa, 390 kPa and 400 kPa were chosen to validate the numerical model, and the related initial settings are listed in Table 2. The fluid temperature of the symmetry axis of the tank was monitored and the temperature comparison between the experimental results T_{exp} and the calculated values T_{cal} is shown in Fig. 2. It is easy to see for different cases, the relative errors of most temperature values are limited in $\pm 20\%$. For few simulated values, the calculation deviation is higher than 20% . It is mainly attributed to the simplify treatment of the calculation model, the additional heat conductions through some connectors are not considered in the simulation. Generally, the fluid temperature of the symmetry axis of the tank is greatly predicted, thus the developed numerical model is acceptable for the following numerical study.

Grid Independence Analysis

With above settings, the tank self-adjustment process after filling is used to conduct the mesh independence research. Four calculation meshes with grid numbers of 21,480, 31,164, 43,698 and 50,920, are selected. As the liquid oxygen is in subcooled statue and the vapor is regional superheated, the tank pressure reduces with time. As Fig. 3 shows, the tank pressure calculated by four meshes has similar reduction profile. Once the grid number increases to 31,164, the calculated pressure has slight variations. From aspects of saving computing resources and improving prediction

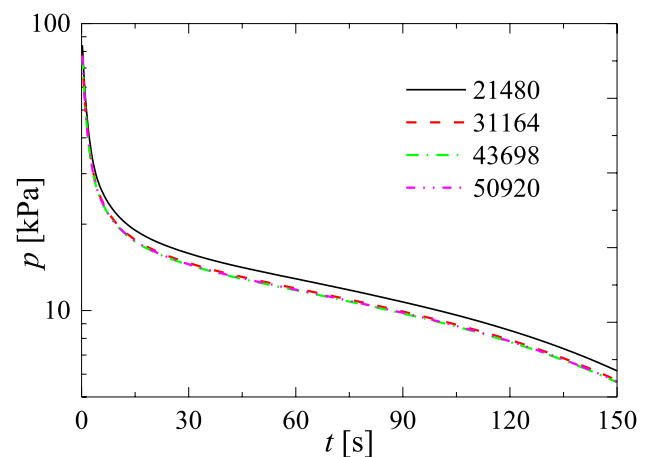


Fig. 3 Comparison of the tank pressure calculated by four meshes

accuracy, the calculation mesh with 43,698 grids is finally selected for the pressurized discharge simulation.

Results and Discussion

Based on above numerical model, the effect of flight acceleration on the pressurization discharge of liquid oxygen from the cryogenic storage tank is investigated. The ground environmental heat invasion is adopted for different cases, and the convection thermal boundary is set with convection heat transfer coefficient of 22 W/(m²K) and air temperature of 293 K. As the flight acceleration ranges from 1g₀ to 5g₀, variations of different parameters are simulated and compared.

Variation of Fluid Pressure

As Fig. 1 shows, 7 pressure test points are set in the symmetry axis of the tank with coordinates of $p_1(0.18,0)$, $p_2(0.68,0)$, $p_3(1.18,0)$, $p_4(1.68,0)$, $p_5(2.18,0)$, $p_6(2.68,0)$ and $p_7(3.18,0)$. Figure 4 shows the pressure distributions of seven test points with $a/g_0=1$. It is easy to see different pressure test points all experience three phases. The first phase lasts for about 30 s, and the liquid filling height ranges in the top elliptical head. During this stage, the fluid pressure has an initial slight increase under the effect of high-temperature gas injection, and then experiences rapid reduction with high rates. Different pressure test points have similar pressure reduction profile. As point p_7 locates in the gas initially, it has a low initial pressure value. With time continuing, pressure profiles of points p_6 and p_7 intersect. Since the intersect point, the pressure value of point p_6 is less than that of point p_7 . This is mainly because with the drop of the liquid filling height, the pressure of point p_6 decreases gradually. As point p_6 is far from the injector, it obtains less energy from the injected gas, compared to point p_7 . Hence, the pressure

of point p_6 is less than that of point p_7 since the first intersect point. As for the phase 2, the liquid filling height varies in the tank cylinder. As the cross-sectional area of the cylinder is larger than that of the top head, the pressure curves of different test points becomes flatter with lower rates, compared to pressure curves in phase 1. Moreover, during the second stage, different pressure profiles also intersect with each other. This is also attributed to the reduction of the liquid filling height. While the test points are surrounded by gas, the test point far from the gas injector has a low pressure value. When the liquid filling height drops into the bottom elliptical head, the cross-sectional area of the free surface has some reductions, so the fluid pressure reduction rate has a corresponding increase. Among different pressure profiles, the profile of point p_1 is independent to other profiles. This is mainly because point p_1 locates in the bottom head and is close to the liquid outlet, so it has higher pressure before the liquid filling height drops to its position.

As for other acceleration conditions, the related pressure distribution profiles are similar to that of $a/g_0=1$ and all experience three phases. Figure 5 displays the pressure distribution of seven test points with $a/g_0=4$. Subjected to higher acceleration, the pressure difference between different pressure points becomes larger and the intersect points among different pressure profiles are more obviously reflected.

The variation of the liquid height h is shown in Fig. 6. It is easy to see h experiences three variation phases. In phase 1, h still locates in the top elliptical head, and reduces with variable rates. While it drops below the top head and varies in the tank cylinder, the tank pressure keeps constant reduction rate. When h reduces to the bottom head, the cross-sectional area of the elliptical head reduces gradually, thus it has a rapid decline with higher reduction rate. As the gas injection flow rate and liquid outflow rate are selected with

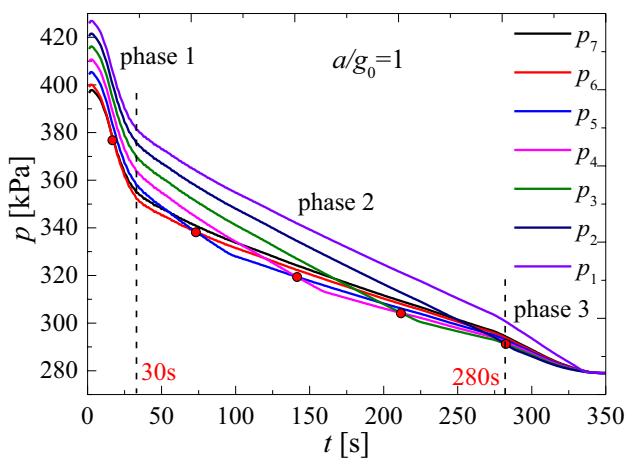


Fig. 4 Pressure variation of different test points with $a/g_0=1$

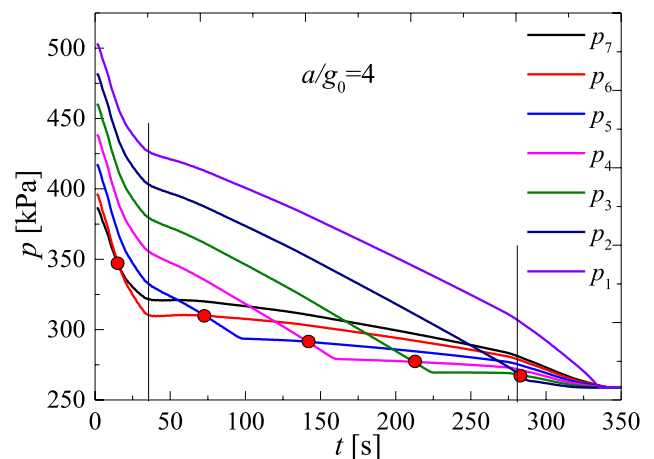


Fig. 5 Pressure variation of different test points with $a/g_0=4$

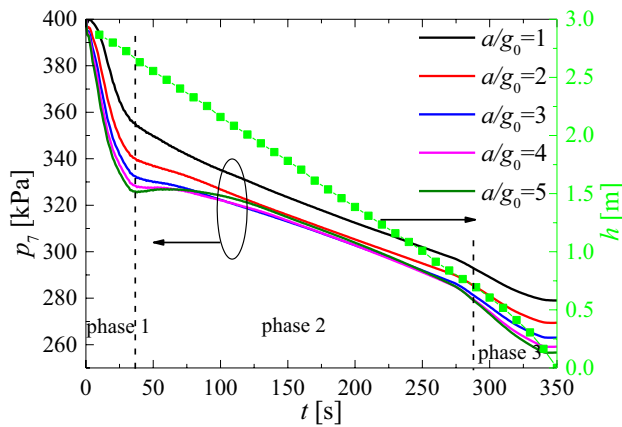


Fig. 6 Variations of the pressure of test point p_7 and liquid height

same values, h have similar variation profile with different acceleration levels.

The drop of h causes obvious variations of fluid pressure. To compare the pressure variation in different accelerations, the pressure profiles of test points p_7 and p_1 are selected and shown in Figs. 6 and 7. It seems that the supergravity level has negative effects on the variation of the gas pressure. As Fig. 6 shows, with a/g_0 ranging from 1 to 3, the pressure of point p_7 reduces with the increase of the acceleration. This is mainly because the flight acceleration promotes the heat exchange from the gas to the liquid and causes the reduction of the gas pressure. While a/g_0 exceeds 3, the gas pressure still decreases with acceleration during phase 1 and phase 3. However, the gas pressure does not have obvious variations in phase 2. The probable reason is that the gas injection has higher moment in higher accelerations, which causes the increase of the gas pressure. The pressure profiles of test point p_1 are shown in Fig. 7. During the first 275 s, the fluid

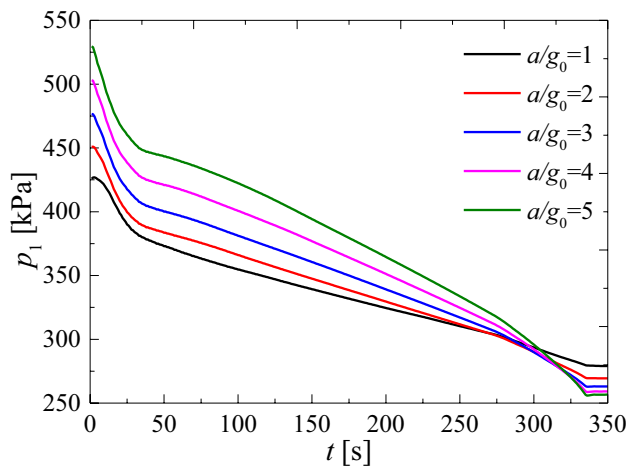


Fig. 7 Pressure variation of test point p_1

pressure increases with the flight acceleration. With time continuing, the pressure of point p_1 in higher acceleration has rapid reductions. Related to the gas pressure, the pressure of point p_1 decreases with acceleration in the last 25 s. Experienced 350 s liquid outflow, the final values of test point p_1 are 279.04 kPa, 269.44 kPa, 263.08 kPa, 259.17 kPa and 256.67 kPa with acceleration varying from $1g_0$ to $5g_0$.

Interface Phase Change

With high-temperature gas injected into the tank, complex heat exchange and phase change occur at the liquid–gas interface. To study the interface phase change phenomenon, both the total mass of gas m_G and the injected mass of gas m_{inject} are monitored, and variations of two parameters are shown in Fig. 8. With the rate of 0.18 kg/s, m_{inject} linearly increases with time. Experienced 350 s liquid discharge, the final value of m_{inject} is 63.0 kg. Under the combination of the interface phase change and gas injection, m_G experiences fluctuating increase in first 300 s, and then has some mass reductions in the later period. Different cases almost have similar variation profiles.

For different cases, the mass increment of gas dm is shown in Fig. 9. It is easy to see dm and m_G have similar variation profile. Moreover, the mass fluctuation amplitude becomes more obvious with the increase of flight acceleration, and dm has negative relation to flight acceleration. When the flight acceleration varies from $1g_0$ to $5g_0$, values of dm are 36.20 kg, 35.66 kg, 34.80 kg, 34.53 kg and 34.25 kg, respectively.

As the mass increment of the gas consists of contributions of the gas injection and interface phase change, so the net phase change capacity could be obtained by comparing dm and m_{inject} . The variation of the interface phase change capacity m_{pc} is calculated and shown in Fig. 10. Caused by

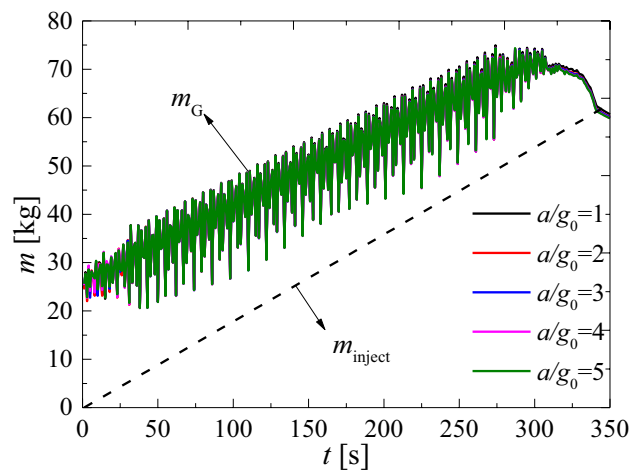


Fig. 8 Variations of the total mass of gas and injected mass of gas

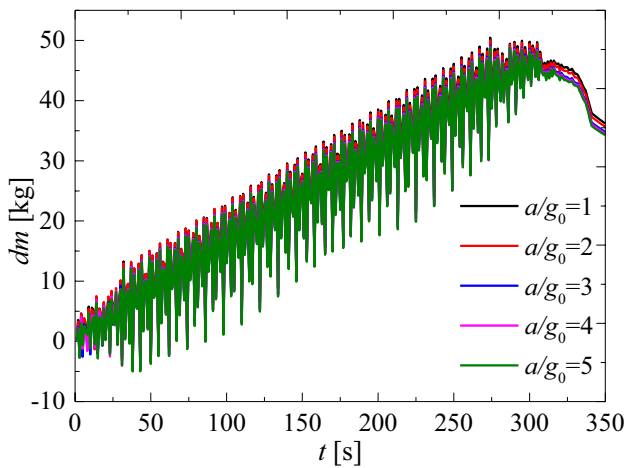


Fig. 9 Variations of the mass increment of gas

the violent interface heat exchange and gas injection, m_{pc} experiences obvious fluctuations and has a gradual reduction trend. While m_{pc} is negative, it means the gas condensation occurs, and while m_{pc} is positive, the liquid evaporates at the interface. In the first 275 s, the phase change mode alters between the liquid evaporation and gas condensation, and the gas condensation is much stronger. Since 275 s, the gas condensation plays the main role during the liquid outflow. The probable causes are given. On the one hand, the reduction of the gas pressure results in the decrease of the saturation temperature, when the gas temperature is lower than the saturation temperature, the gas condensation occurs. On the other hand, the gas has a higher temperature, and it conducts thermal capacity to outside through the tank wall, and finally causes the gas condensation. Combing Figs. 9 and 10, it seems that the lower mass increment and larger gas condensation forms in higher acceleration condition. After

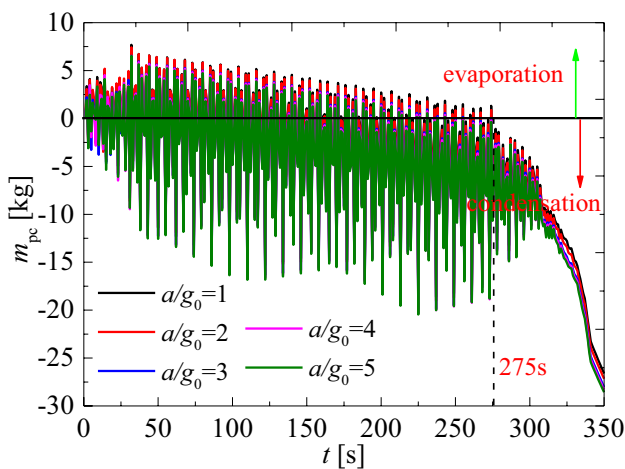


Fig. 10 Variations of the phase change capacity

350 s pressurization discharge, the final values of m_{pc} are -26.62 kg, -27.16 kg, -28.02 kg, -28.29 kg and -28.57 kg, respectively.

Fluid Temperature Distribution

The fluid thermal stratification and phase distribution with accelerations of $1g_0$, $3g_0$ and $5g_0$, are selected and shown in Fig. 11. The fluid temperature is limited from 80 to 360 K. As Fig. 11 shows, the thermal stratification develops greatly in the gas region. Subjected to gas injection, the heat exchange between the gas and the interface is promoted. While 360 K high-temperature gaseous oxygen is injected, the gas is heated and the heated gas moves upwards driven by thermal buoyancy. The high temperature region forms in the up elliptical head and its district decreases with flight acceleration. Influenced by the gas pressure, the fluid temperature distribution near the gas injector are different. In the liquid region, the fluid stratification is not obviously reflected because of small temperature increase. For the liquid far from the interface, it almost maintains the initial liquid temperature without obtaining heat capacity from high-temperature gas.

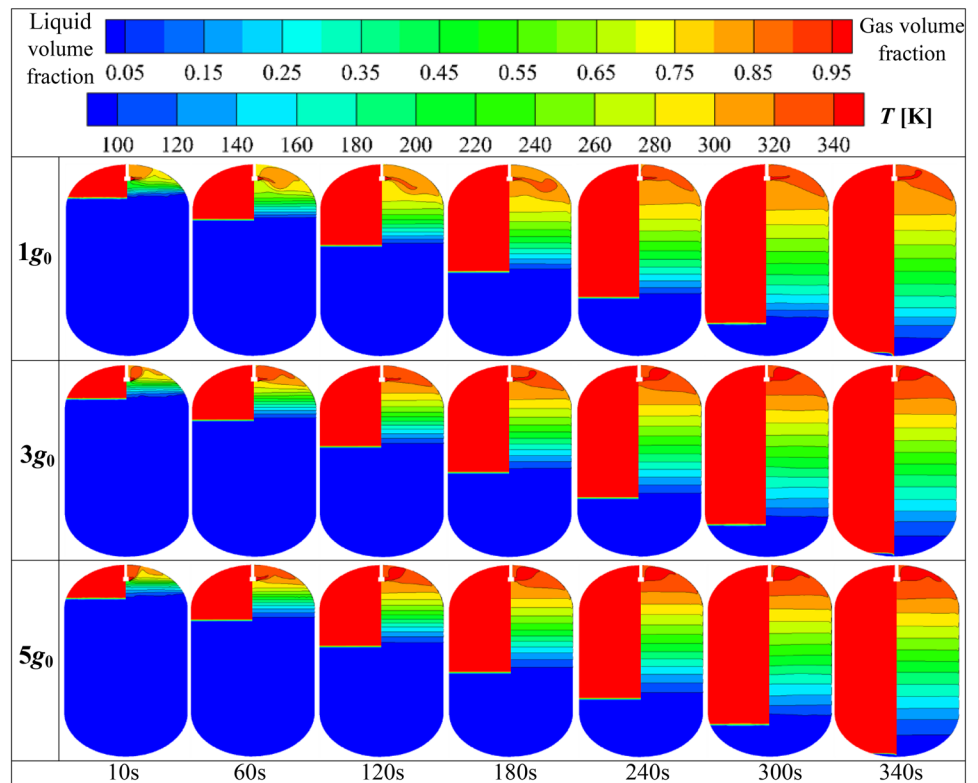
As for the phase distribution, obvious interface forms in different cases. The effect of the gas injection on the interface disturbance only appears in the initial stage and fades away with time continuing. Moreover, the drop of h is also reflected by the phase distribution. With the fluid outflow, h almost linearly decreases in the first 320 s, and experiences rapid reduction in the last 30 s.

To clearly display fluid temperature history during the liquid outflow, three temperature test points are set with coordinates of $T_1(0.18,0)$, $T_3(1.18,0)$ and $T_5(2.18,0)$. As the flight acceleration largely promotes the heat exchange from the high-temperature gas to the liquid, the high-temperature gas is greatly cooled by the subcooled liquid. Therefore, the gas of higher acceleration has a lower temperature. Before h drops to these three test points, the liquid temperature almost keeps constant. While the liquid height reduces to positions of these test points, the gas temperature are displayed. As Fig. 12 shows, once the test points are exposed to the gas, their temperatures increase gradually with time and decrease with flight acceleration.

Interface Fluid and Outflow Performance

Both the interface pressure p_{inter} and fluid temperature T_{inter} are monitored during liquid outflow. Figure 13 shows the interface fluid pressure variation in different conditions. It is easy to see p_{inter} always experiences three phases with h varying in top head, cylinder and bottom head. Compared to the pressure test point p_7 , the liquid–gas interface is far from the gas injector, so the interface has a lower initial

Fig. 11 Fluid temperature distribution (right side) and phase distribution (left side) in different cases



pressure. Generally, p_{inter} decreases with flight acceleration. During 350 s pressurization discharge, the final vales of p_{inter} are 279.27 kPa, 269.68 kPa, 263.32 kPa, 259.43 kPa and 256.93 kPa, respectively.

The saturation temperature T_{SAT} corresponding to p_{inter} is shown in Fig. 14. It is easy to see T_{SAT} has similar variation profiles to p_{inter} and experiences three temperature reduction phases. Moreover, T_{SAT} decreases with the increase of the gravity acceleration level, and its values are always higher than 100 K.

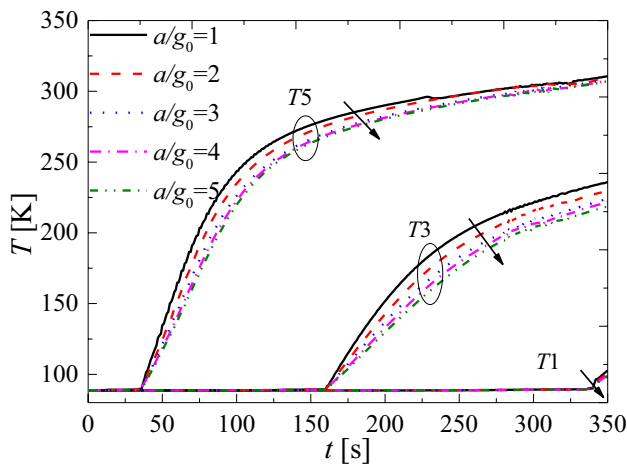


Fig. 12 Temperature variations of four test points

The interface fluid temperature T_{inter} is also calculated and the related temperature variations are shown in Fig. 14. Different from p_{inter} and T_{SAT} , T_{inter} experiences fluctuating variations. The main reason is given. During the initial period, h is high and the interface is close to the gas injector, T_{inter} is largely influenced by the high-temperature gas injection. With time continuing, the effect of the initial gas injection fades away, and the fluctuation of T_{inter} is mainly caused by the violent interface phase change. Moreover, directly

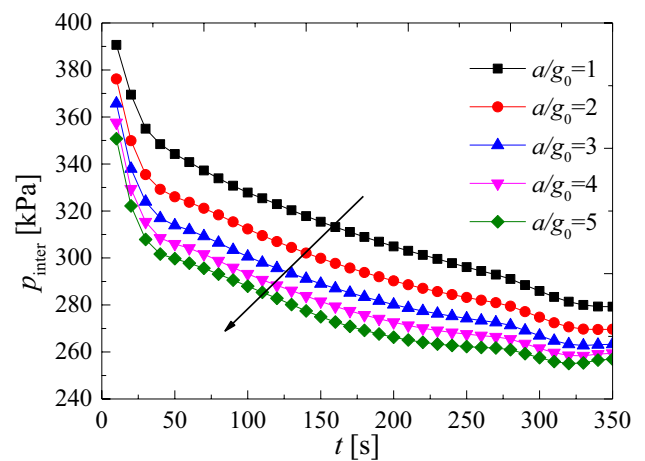


Fig. 13 Variations of the interface fluid pressure

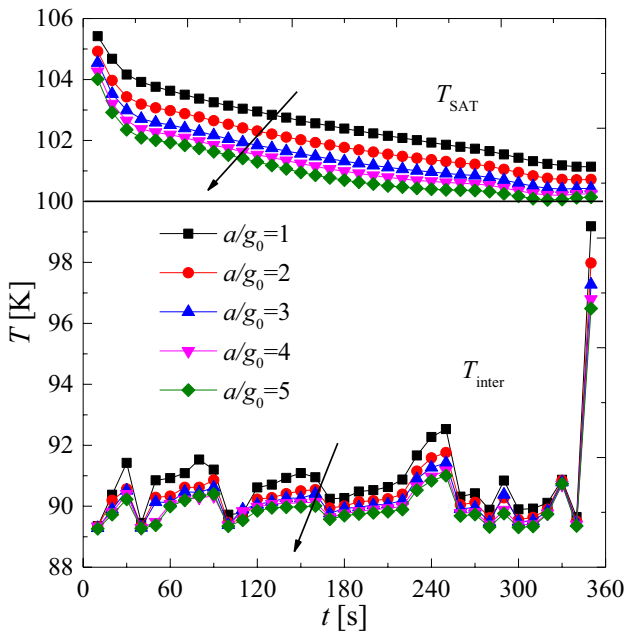


Fig. 14 Variations of the interface fluid temperature and saturation temperature

related to p_{inter} , T_{inter} also decreases with gravity acceleration. Moreover, it is evident to find that T_{inter} is always lower than T_{SAT} . Based on above phase change model, the gas condensation will occur at the liquid–gas interface. Actually, it is T_{inter} that determines the interface phase change process. Influenced by the fluctuation variation of T_{inter} , both the liquid evaporation and gas condensation occur at the interface. Moreover, as the higher gravity acceleration promotes the heat transfer from the gas to the liquid, so the gas condensation capacity increases with flight acceleration, which is consistent with results shown in Fig. 10.

The fluid outflow performance is investigated by monitoring the outflow pressure p_{out} and fluid temperature T_{out} at the outlet with coordinate $Z=0$. As Fig. 15 shows, p_{out} experiences three phases and has gradual reducing profile. As the liquid static pressure increases with flight acceleration, the initial outflow pressure has larger values for higher acceleration. p_{out} increases with flight acceleration in the first 330 s. With the drop of h and decrease of the gas pressure, p_{out} has obvious reduction. Since 330 s, p_{out} decreases with flight acceleration. By comparing Figs. 7 and 15, it is easy to find that p_{out} has similar variation profile to the test point p_1 .

The saturation temperature T_{SAT} corresponding to p_{out} is shown in Fig. 16. It is clear to see T_{SAT} has similar variation profile to p_{out} , and its values are always higher than 100 K for different conditions. The temperature variation of the outflow liquid is also monitored. As Fig. 16 shows, the outflow liquid experiences an initial temperature constancy or slight temperature reduction in the first 200 s. Afterwards,

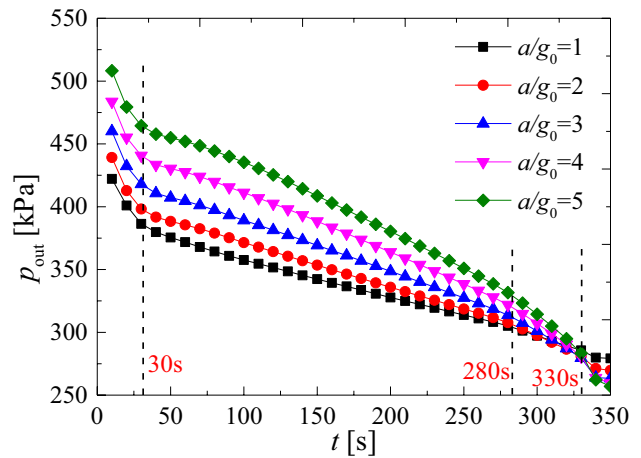


Fig. 15 Variations of the outflow fluid pressure

T_{out} experiences rapid increase. As for the initial temperature reduction, it is mainly because the subcooled liquid mixtures with the heated fluid subjected to external environmental heat invasion, which causes the slight temperature decrease of the outflow liquid. As the interface fluid obtains more thermal energy from the gas and external environment, a thermal stratified layer forms below the interface. With the drop of the liquid height, the thermal layer is close to the outlet and conducts more thermal energy downward, so the outflow fluid has obvious temperature increase. Experienced

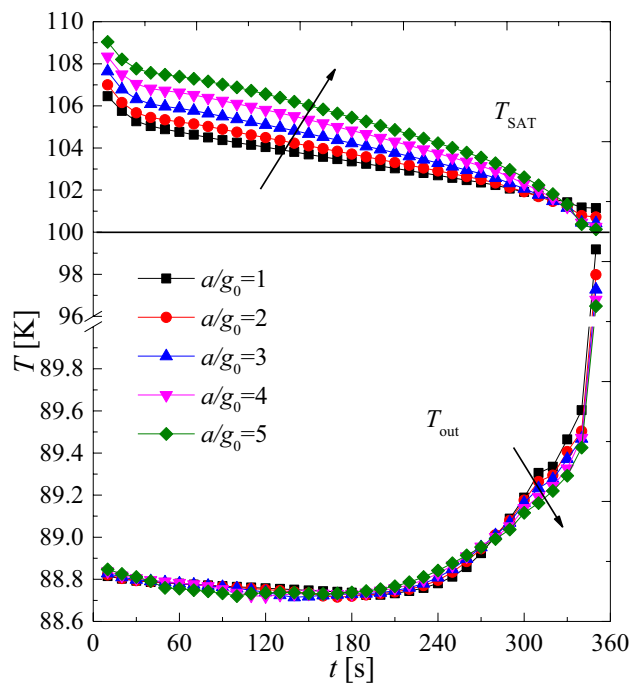


Fig. 16 Variations of the outflow fluid temperature and saturation temperature

350 s liquid outflow, the final values of T_{out} are 99.18 K, 97.98 K, 97.28 K, 96.79 K and 96.49 K, with acceleration ranging from $1g_0$ to $5g_0$. Moreover, the values of T_{out} are lower than that of T_{SAT} for different conditions. That is to say obvious liquid boil-off generation does not form at the outlet, and this phenomenon is consistent with the phase change capacity shown in Fig. 10.

Conclusions

A numerical simulation on the pressurization discharge of liquid oxygen from a cryogenic storage tank is conducted. With the gas injection flow rate of 0.18 kg/s and the liquid outflow rate of 36.0 kg/s, the effect of the flight acceleration is numerically researched on the liquid outflow performance. Some main conclusions are obtained.

1. Different pressure test points all experience three pressure reduction phases. The intersection point forms between any two pressure profiles. Generally, the gas pressure decreases with flight acceleration. However, caused by the gas injection and interface phase change, the gas pressure of high acceleration level may be higher than that of low acceleration level. Influenced by the hydrostatic pressure, the liquid pressure increases with flight acceleration. With the drop of the liquid height, most of test points are exposed to the gas, and the pressure of test points starts to decrease with flight acceleration.
2. Influenced by the gas injection, the total mass of gas experiences fluctuation variations in the first 300 s, and then experiences rapid decline in the later period. The mass increment of gas decreases with flight acceleration. Both the gas condensation and liquid evaporation occur at the interface in the first 275 s, and then the gas condensation becomes the main phase change mode. As high acceleration promotes the heat conduction from the gas to the interface, the gas condensation capacity increases with flight acceleration.
3. Fluid thermal stratification develops greatly in gas region. The thermal stratified layer forms below the interface. With the drop of the liquid height, the gas temperature increases with time. As the acceleration promotes the heat exchange between the gas to the liquid, the gas temperature of higher acceleration condition has a lower value. That is to say when the test point is exposed to the gas, the gas temperature decreases with flight acceleration.
4. The interface fluid pressure decreases with flight acceleration. Influenced by the gas injection and violent phase change, the interface fluid temperature experiences fluctuation variations.

The interface fluid temperature experiences fluctuation variations. The outflow pressure increases with flight acceleration in the first 330 s. While the effect of the gas pressure becomes prominent, the outflow pressure decreases with flight acceleration in the last 20 s. The temperature of the outflow fluid experiences relative stable variations in the first 200 s, and then increases rapidly. The final fluid temperature decreases with flight acceleration. There is no obvious liquid boil-off generation at the outlet for different conditions.

Based on above discussions, it is easy to see the higher acceleration usually causes obvious gas condensation and gas pressure reduction. To reduce the obvious decline of the tank pressure and maintain the safety operation of cryogenic fuel storage tanks, parameters on the gas injection and liquid outflow should be properly designed and optimized.

Nomenclature

a : Flight acceleration, ms^{-2} ; c_p : Special heat at constant pressure, $\text{J kg}^{-1} \text{K}^{-1}$; Cr : Courant number; dm : Mass increment, kg ; E : Internal energy, J kg^{-1} ; \vec{F}_{vol} : Volume force vector; g_0 : Normal gravity acceleration, 9.81 ms^{-2} ; \vec{g} : Gravity vector; h : Height, m ; h_{fg} : Latent heat, J kg^{-1} ; k : Turbulent kinetic energy; l : Characteristic length, m ; m : Mass, kg ; p : Pressure, Pa ; Pr : Prandtl number; q : Heat flux, Wm^{-2} ; r : Mass transfer intensity factor, s^{-1} ; Ra^* : Modified Rayleigh number; S_h : Energy source term, Wm^{-3} ; S_m : Mass source term, $\text{kg m}^{-3} \text{s}^{-1}$; t : Time, s ; T : Thermodynamic temperature, K ; \vec{v} : Velocity vector; α : Volume fraction and heat transfer coefficient, $\text{Wm}^{-2} \text{K}^{-1}$; β : Thermal expansion coefficient, K^{-1} ; λ : Thermal conductivity, $\text{Wm}^{-1} \text{K}^{-1}$; μ : Dynamic viscosity, Pa s ; ν : Kinematic viscosity, $\text{m}^2 \text{s}^{-1}$; ρ : Density, kg m^{-3} ; ϵ : Turbulent kinetic energy dissipation

Subscripts

cal: Calculation; exp: Experiment; G: Gas; inject: Injected; inter: Interface; L: Liquid; out: Outflow; pc: Phase change; q: Liquid or gas phase.; SAT: Saturation

Acknowledgements This work was supported by the National Natural Science Foundation of China (51806235) and the Research Fund of State Key Laboratory of Technologies in Space Cryogenic Propellants (SKLTSCP202109). The first author is grateful to the China Scholarship Council (CSC) for funding his oversea study (Grant No. 202006425010). The authors are also grateful to the open access funding for this research paper provided by Lund University.

Funding Open access funding provided by Lund University.

Declarations

Competing Interest The authors declare that they have no known competing financial interests or personal relationships that could have appeared to influence the work reported in this paper.

Open Access This article is licensed under a Creative Commons Attribution 4.0 International License, which permits use, sharing, adaptation, distribution and reproduction in any medium or format, as long as you give appropriate credit to the original author(s) and the source, provide a link to the Creative Commons licence, and indicate if changes were made. The images or other third party material in this article are included in the article's Creative Commons licence, unless indicated otherwise in a credit line to the material. If material is not included in the article's Creative Commons licence and your intended use is not permitted by statutory regulation or exceeds the permitted use, you will need to obtain permission directly from the copyright holder. To view a copy of this licence, visit <http://creativecommons.org/licenses/by/4.0/>.

References

- Aydelott, J.C.: Normal gravity self-pressurization of 9-inch-(23cm) diameter spherical liquid hydrogen tankage. Washington, D.C.: NASA Technical Note, NASA TN D-4171 (1967a)
- Aydelott, J.C.: Effect of gravity of self-pressurization of spherical liquid-hydrogen tankage. Cleveland: Lewis Research Center (1967b)
- Barsi, S., Kassemi, M.: Numerical and experimental comparisons of the self-pressurization behavior of an LH2 tank in normal gravity. *Cryogenics* **48**(3–4), 122–129 (2008)
- Chen, X., Qi, C., Wang, W., Miao, J., Zhang, H.: Theoretical Analysis of Cryogenic Fluid Evaporation in Sintered Microporous Structures. *Microgravity Sci. Technol.* **34**(2), 1–20 (2022)
- Hearn, H.C.: Development and validation of fluid/thermodynamic models for spacecraft propulsion systems. *J. Propul. Power* **17**(3), 527–533 (2001)
- Hochstein, J.I., Jit, H.C., Aydelott, J.C.: Prediction of self-pressurization rate of cryogenic propellant tankage. *J. Propul. Power* **6**(1), 11–17 (1990)
- Inoue, K., Ohta, H., Asano, H., Kawanami, O., Imai, R., Suzuki, K., Shinmoto, Y., Matsumoto, S.: Heat Loss Analysis of Flow Boiling Experiments Onboard International Space Station with Unclear Thermal Environmental Conditions (2nd Report: Liquid-vapor Two-phase Flow Conditions at Test Section Inlet). *Microgravity Sci. Technol.* **33**(5), 1–14 (2021)
- Lee, W.H.: A pressure iteration scheme for two-phase flow modeling. In: *Multiphase Transport: Fundamentals, Reactor Safety, Applications*. 407–432 (1980)
- Li, J., Liang, G., Zhu, P., Wang, X.: Numerical investigation of the operating process of the liquid hydrogen tank under gaseous hydrogen pressurization. *Aerosp. Sci. Technol.* **93**, 105327 (2019)
- Li, J.C., Guo, B., Zhao, J.F., Li, K., Hu, W.R.: On the Space Thermal Destratification in a Partially Filled Hydrogen Propellant Tank by Jet Injection. *Microgravity Sci. Technol.* **34**(1), 1–25 (2022)
- Liu, Z., Chen, H., Chen, Q., Chen, L.: Numerical Study on thermodynamic performance in a cryogenic fuel storage tank under external sloshing excitation. *Int. J. Aeronaut. Space Sci* **22**(5), 1062–1074 (2021)
- Liu, Z., Feng, Y., Lei, G., Li, Y.: Hydrodynamic performance in a sloshing liquid oxygen tank under different initial liquid filling levels. *Aerosp. Sci. Technol.* **85**, 544–555 (2019a)
- Liu, Z., Feng, Y., Cui, J., Lei, G., Li, Y.: Effect of excitation types on sloshing dynamic characteristics in a cryogenic liquid oxygen tank. *J. Aerosp. Eng.* **32**(6), 04019096 (2019b)
- Liu, Z., Feng, Y., Yan, J., Li, Y., Chen, L.: Dynamic variation of interface shape in a liquid oxygen tank under a sinusoidal sloshing excitation. *Ocean Eng.* **213**, 107637 (2020a)
- Liu, Z., Feng, Y., Lei, G., Li, Y.: Thermal physical process in a liquid oxygen tank under different sloshing excitations. *Int. Commun. Heat Mass Transfer* **117**, 104771 (2020b)
- Liu, Z., Li, C.: Influence factors of the numerical model build-up on fluid sloshing. *Exp. Comput. Multiph. Flow* (2021). <https://doi.org/10.1007/s42757-020-0099-6>
- Liu, Z., Li, Y., Jin, Y.: Pressurization performance and temperature stratification in cryogenic final stage propellant tank. *Appl. Therm. Eng.* **106**, 211–220 (2016)
- Liu, Z., Li, Y., Jin, Y., Li, C.: Thermodynamic performance of pre-pressurization in a cryogenic tank. *Appl. Therm. Eng.* **112**, 801–810 (2017)
- Liu, Z., Pan, H., Liu, Y., Li, Y.: Thermodynamic performance on the pressurized discharge process from a cryogenic fuel storage tank. *Int. J. Hydrog. Energy* **47**, 12107–12118 (2022)
- Ludwig, C., Dreyer, M.E.: Investigations on thermodynamic phenomena of the active-pressurization process of a cryogenic propellant tank. *Cryogenics* **63**, 1–16 (2014)
- Majumdar, A., Steadman, T.: Numerical modeling of pressurization of propellant tank. *J. Propul. Power* **17**(2), 385–390 (2001)
- Mandell, D.A., Roudebush, W.H.: Parametric investigation of liquid hydrogen tank pressurization during outflow. Cleveland: Lewis Research Center (1965)
- Mao, H., Li, Y., Huang, X., Xia, S., Sundén, B.: Investigation on the elimination of geyser in a cryogenic pipe by a recirculation method. *Appl. Therm. Eng.* **197**, 117428 (2021)
- NIST Chemistry WebBook: NIST standard reference database. October 2011 release, available from: <http://webbook.nist.gov/chemistry/>. (2011)
- Panzarella, C.H., Kassemi, M.: Self-pressurization of large spherical cryogenic tanks in space. *J. Spacecr. Rocket.* **42**(2), 299–308 (2005)
- Roudebush, W.H.: An analysis of the problem of tank pressurization during outflow. Cleveland: Lewis Research Center, (1965)
- Seo, M., Jeong, S.: Analysis of self-pressurization phenomenon of cryogenic fluid storage tank with thermal diffusion model. *Cryogenics* **50**(9), 549–555 (2010)
- Stochl, R.J.: Gaseous helium requirements for the discharge of liquid hydrogen from a 1.52 meter diameter spherical tank. Cleveland: Lewis Research Center, (1970a)
- Stochl, R.J., Maloy, J.E.: Gaseous helium requirements for the discharge of liquid hydrogen from a 3.96 meter diameter spherical tank. Cleveland: Lewis Research Center, (1970b)
- Stochl, R.J., Masters, P.A., DeWitt, R.L., Stochl, R.J.: Gaseous hydrogen requirements for the discharge of liquid hydrogen from a 1.52 meter diameter spherical tank. Cleveland: Lewis Research Center, (1969)
- Suñol, F., Ochoa, D.A., Granados, M., González-Cinca, R., García, J.E.: Performance assessment of ultrasonic waves for bubble control in cryogenic fuel tanks. *Microgravity Sci. Technol.* **32**(4), 609–613 (2020)
- Van Dresar, N.T., Stochl, R.J.: Pressurization and expulsion of cryogenic liquid generic requirements for a low gravity experiment. Cleveland: Lewis Research Center, (1991)
- Van Dresar, N.T., Stochl, R.J.: Pressurization and expulsion of a flight weight liquid hydrogen tank. Cleveland: Lewis Research Center, (1993)
- Wang, B., Qin, X., Jiang, W., Li, P., Sun, P., Huang, Y.: Numerical simulation on interface evolution and pressurization behaviors in cryogenic propellant tank on orbit. *Microgravity Sci. Technol.* **32**(1), 59–68 (2020)
- Wang, L., Li, Y., Jin, Y., Ma, Y.: Experimental investigation on pressurization performance of cryogenic tank during high-temperature helium pressurization process. *Cryogenics* **66**(3), 43–52 (2015)

- Wang, L., Li, Y., Zhao, Z., Liu, Z.: Transient thermal and pressurization performance of LO2 tank during helium pressurization combined with outside aerodynamic heating. *Int. J. Heat Mass Transf.* **62**(7), 263–271 (2013)
- Wickert, D., Prokop, G.: Simulation of water evaporation under natural conditions—A state-of-the-art overview. *Exp. Comput. Multiph. Flow* **3**(4), 242–249 (2021)

Publisher's Note Springer Nature remains neutral with regard to jurisdictional claims in published maps and institutional affiliations.